

The Continuous p -Dispersion Problem in Three Dimensions

Sanjay Manoj¹ and Melkior Ornik¹

¹*University of Illinois Urbana-Champaign*

Abstract: The Continuous p -Dispersion Problem (CpDP) with boundary constraints asks for the placement of a fixed number of points in a compact subset of Euclidean space such that the minimum distance between any two points, as well as the points and the boundary of this compact set is maximized. This problem finds applications in facility placement, communication network design, sampling theory, and particle simulation; however, finding optimal solutions is NP-hard and existing algorithms focus on providing approximate solutions in two-dimensional space. In this paper, we introduce an almost-everywhere differentiable optimization model and global optimization algorithm for approximating solutions to the CpDP with boundary constraints in convex and non-convex polyhedra with respect to any metric in a three-dimensional Euclidean space. Our algorithm generalizes two-dimensional dispersion techniques to three dimensions by leveraging orientation, linear-algebraic projections for point-to-face distances, and a ray-casting procedure for point-in-polyhedron testing, enabling optimization in arbitrary convex and non-convex three dimensional polyhedra. We validate the proposed algorithm by comparing with analytical optima where available and empirical benchmarks, observing close agreement with optimal solutions and improvements over empirical benchmarks.

I. INTRODUCTION

In 1987, Kuby [1] proposed the p -Dispersion Problem, asking to locate p facilities on a network so that the minimum separation distance between any pair of open facilities is maximized. Later in 1995, Drezner and Erkut [2] formalized the p -Dispersion Problem, asking for the placement of p points from a subset of \mathbb{R}^n such that the minimum distance between pairs of points is maximized. Subsequently, the Continuous p -Dispersion Problem (CpDP) with boundary constraints adds the requirement that a dispersion point must be sufficiently far away from the boundary of the subset of \mathbb{R}^n , also often referred to as a container. The p -Dispersion Problem is interesting because it formalizes the inherent trade-off between coverage and separation, to find how a limited number of points can be optimally distributed over a domain. The p -Dispersion problem is provably NP-complete for the general container [3] in the number of dispersion points p .

Existing work solving the p -Dispersion problem primarily focuses on low-dimensional containers with special geometric properties. For instance, repulsion-based heuristics have been applied to circular containers [4] and non-convex two-dimensional polygons [5]. Other approaches include a 2/3-approximation algorithm for rectilinear polygons [3] and a Tabu Search Global Optimization (TSGO) algorithm for general planar containers [6]. In higher dimensions, work is severely limited: Drezner and Erkut [2] formulated a nonlinear model restricted to the unit square, while Kazakov et al. [7] developed a grid-based sphere-packing algorithm that struggles with complex, non-convex three-dimensional boundaries.

Compared to previous work, the goal of this paper is to approximate elements of the solution set for the CpDP within general polyhedral containers with respect to any metric in \mathbb{R}^3 [6]. The TSGO algorithm proposed by Lai et al. [6] is difficult to adapt to higher dimensions

because it is built around two-dimensional logic. Their model relies on measuring distances to the edges of a polygon and uses repeated point-in-polygon tests to check for constraint violations. We extend this approach to solve the CpDP for general polyhedral containers in three dimensions. Our method uses a ray-casting procedure for point-in-container testing and replaces their edge-based distance checks with a formulation that calculates the distance to the faces, edges, and vertices of the three-dimensional boundary.

Solving the CpDP in three dimensions reflects how spatial dispersion is performed in real-world situations where objects have volume and operate in bounded physical space, such as collision avoidance for autonomous agents [8] or transmitter placement in complex indoor environments [9]. Importantly, the mathematical abstractions based on [6] established in this work are designed to be extensible to general n -dimensional containers. While the primary challenge in such a transition lies in the geometric modeling of arbitrary high-dimensional polyhedra, containers with uniform constraints, such as an n -dimensional hypercube with limits restricted between 0 and 1, remain straightforward to model within this framework. We build on the work from Lai et al. [6] by defining a feasibility-residual function to approximately solve the CpDP with boundary constraints for convex and non-convex polyhedral containers in \mathbb{R}^3 . A feasibility-residual function $E(x) = 0$ if and only if x is feasible solution, and $E(x) > 0$ otherwise. To minimize this function, we utilize the Tabu Search heuristic [10] which improves upon standard local searches by marking previously visited configurations as "tabu" to prevent cycling and encourage the exploration of more optimal regions of the solution space [6].

We also generalize the Continuous p -Dispersion Problem by allowing the distance between points and the boundary to be measured using a metric. This allows the algorithm to handle separation constraints defined by general shapes—like cubes or octahedra—rather than being

limited to standard spherical constraints. This change broadens the types of dispersion problems the algorithm can solve and provides a single framework for optimizing point layouts under different geometric requirements. We validate our algorithm’s accuracy by comparing its results against optimal results in the unit cube proven by Schaefer [11], measuring the relative deterioration to show how closely our algorithm approaches global maxima. For non-rectangular containers, we benchmark our results against the best-known packings for the unit tetrahedron provided by Kazakov et al. [7]. We also establish new results for non-convex polyhedra and provide visualizations for our best-achieved configurations in several containers.

Basic Notation: We use the following standard notation throughout this paper. Let $d(\cdot, \cdot)$ denote a metric on \mathbb{R}^n following the usual definition [12]. The distance between an element $x \in \mathbb{R}^3$ and a nonempty subset $X \subseteq \mathbb{R}^3$ is given by $d(x, X) = \inf\{d(x, y) : y \in X\}$. The *open ball* and *closed ball* of radius r centered at x are defined as $B_r^o(x) = \{y \in \mathbb{R}^3 : d(x, y) < r\}$ and $B_r^c(x) = \{y \in \mathbb{R}^3 : d(x, y) \leq r\}$, respectively. For any positive integer n , let $[n] = \{1, \dots, n\}$. Finally, for a subset $X \subseteq \mathbb{R}^3$, ∂X denotes the boundary of X , $X^c = \mathbb{R}^3 \setminus X$ is the complement of X , and $X^\circ = X \setminus \partial X$ is the interior of X .

II. PROBLEM FORMULATION

The Continuous p -Dispersion Problem (CpDP) asks to place p points, i.e., *sites*, within a compact subset, i.e., a *container*, in \mathbb{R}^n so that the minimum pairwise distance between the sites is maximized [2]. A variation on the CpDP includes “boundary constraints” which asks that the minimum distance between any two points, as well as the points and the boundary of this compact set be maximized [3]. Most existing algorithms that solve the CpDP do so in the setting of bounded, polygonal containers in two dimensions, possibly with holes. In the three dimensions, the natural extension is to consider bounded containers which are polyhedra with polyhedral holes. A *polyhedron* is a closed and bounded solid C whose boundary ∂C can be covered by finitely many planes [13]. A *polyhedral container* is a polyhedron C with holes $U_1, \dots, U_k \subseteq C$ which are also polyhedra.

We denote $C = (V, E, F)$ where V is the set of vertices of C , E is the set of edges of C and F is the set of faces of C . We require that the interior of a polyhedral container be non-empty, therefore providing the polyhedral container with a consistent orientation with inward normals [14]. We write $x \in C$ for an element $x \in \mathbb{R}^3$ inside the polyhedron but outside its holes. An element $x \notin C$ is located outside the polyhedron or inside the polyhedral container’s holes.

We now state the Continuous p -Dispersion Problem (CpDP) [2] with boundary constraints for polyhedral containers with respect to any metric d on \mathbb{R}^3 .

Problem: Let $p \in \mathbb{N}$ and $C \subseteq \mathbb{R}^3$ be a polyhedral container. We solve the nonlinear optimization problem:

$$\begin{aligned} & \max_{c_1, \dots, c_p} D \\ \text{subject to } & c_1, \dots, c_p \in C, & (i) \\ & d(c_i, c_j) \geq 2D \text{ for all distinct } i, j \in [p], & (ii) \\ & d(c_i, \partial C) \geq D \text{ for all } i \in [p]. & (iii) \end{aligned}$$

Note that we will interpret the value of D to be the radius of the ball centered at each dispersion point c_i . For a feasible solution $(c_1, \dots, c_p, D) \in (\mathbb{R}^3)^p \times \mathbb{R}$ to the nonlinear optimization problem, we refer to the elements $c_i \in \mathbb{R}^3$ as *dispersion points* and $D \in \mathbb{R}_{>0}$ as the *radius* of the solution. A *configuration* (of dispersion points) X refers to the set $X = \{c_1, \dots, c_p\}$ for a given feasible solution.

These constraints enforce three geometric requirements: (i) the *containment constraint* ensures each point c_i lies within the container; (ii) the *dispersion constraint* requires mutual separation, meaning $B_D^o(c_i) \cap B_D^o(c_j) = \emptyset$ for all distinct $i, j \in [p]$; and (iii) the *boundary constraint* keeps points away from the edges, ensuring $B_D^o(c_i) \cap \partial C = \emptyset$ for all $i \in [p]$.

From the assumption that the interior of the container C is nontrivial, a feasible solution (c_1, \dots, c_p, D) always exists [5].

The CpDP is hard to attack naively due to the massive number of non-convex feasible sets of the nonlinear program. As a result, standard nonlinear optimizers often get caught in local minima. Additionally, the number of distance constraints to compute is $\binom{p}{2} = \mathcal{O}(p^2)$, and with minimum distance bounds, it is highly likely that a random initial configuration will violate the dispersion constraint (ii).

III. OPTIMIZATION MODEL

In this section we introduce a unified feasibility-residual function used to solve the CpDP with boundary constraints by modeling constraint violation in two parts: *dispersion violation* and *container violation*. Dispersion violation stems from dispersion points being located too close together; namely, when $d(c_i, c_j) < 2D$ for some fixed $D > 0$, constraint (ii) is violated. Container violation is a result of dispersion points being located too close to the boundary of the container; namely, when $d(c_i, \partial C) < D$ for some fixed $D > 0$, constraint (iii) is violated.

By combining these two components into a single feasibility-residual function, we can address inherent geometric complexities associated with any container. In general, the feasible region for the solution set to the CpDP is non-convex. Moreover, as the number of dispersion points p increases, the feasible region will contain many local optima [6].

Lai et al. [6] proposed a novel framework for the two-dimensional CpDP by unifying dispersion and boundary

constraints into a single, non-negative feasibility-residual function, E_D . They conceptualized constraint violations as *energy*, where the total energy of a configuration corresponds to its distance from feasibility. For a configuration of points $X \in (\mathbb{R}^2)^p$ and fixed $D \geq 0$, this function

is defined as $E_D(X) = \sum_{i=1}^{p-1} \sum_{j=i+1}^p \ell_{ij}^2 + \sum_{i=1}^p O_i$ where ℓ_{ij} is

the dispersion penalty between points c_i and c_j , and O_i is the boundary penalty for point c_i . A crucial property of this formulation is that $E_D(X) = 0$ if and only if (X, D) is a feasible solution. Because E_D is almost-everywhere differentiable, it allows for the application of efficient gradient-based optimization methods, such as the Limited-memory Broyden-Fletcher-Goldfarb-Shanno (L-BFGS) algorithm [15]. This approach proved exceptionally powerful, enabling the rapid convergence to local optima from random initial configurations.

Extending the optimization model from Lai et al. [6] to three dimensions introduces several significant challenges. While the dispersion penalty term is easy enough to compute in any finite number of dimensions, computing the boundary penalty term in three dimensions becomes computationally complex. First, Lai et al. [6] defines their boundary constraint term in a manner which heavily relies on planar geometry where counter-clockwise traversal of closed polygonal loops provides a canonical way to distinguish the interior from the exterior. We generalize boundary orientation of polygonal containers from two-dimensional vertex traversal to three dimensions by orienting the faces of the polyhedron using inward normals. By assigning an inward-pointing normal to each face, we explicitly define the interior half-space of the polyhedron. In our algorithm, these normals serve as the directional basis for calculating distance-to-boundary terms for dispersion points and performing feasibility checks.

Additionally, point-in-container testing is fundamental to the boundary constraint term, as it dictates whether to apply a repulsive force to maintain interiority or an attractive force to recover feasibility from the exterior. While point-in-polygon testing admits efficient deterministic routines [16], no such efficient subroutines are devised for three-dimensional containers that scale well with the number of vertices. Consequently, we utilize a ray-casting-based point-in-polyhedron procedure [17] together with the polyhedron's orientation to create projection-based distance calculations which handle complex or non-convex polyhedral containers. The ray-casting procedure draws multiple rays in a random directions from a given dispersion point and counts the number of faces it intersects. If a given ray intersects an even number of faces, the dispersion point is categorized as exterior; an odd number of intersections identifies the point as interior. Because rays may occasionally strike a vertex or edge leading to numerical ambiguity, we cast multiple rays and employ a majority-voting scheme to ensure a robust classification. These geometric tools provide the foundation needed to

extend the underlying optimization model to three dimensions.

With this geometric framework in place, we now adapt the optimization model presented in Lai et al. [6] to three dimensions. The *energy of a solution* (c_1, \dots, c_p, D) will be measured by its quantification of constraint violation. Recall that high energy solutions have a high degree of constraint violation and low energy solutions have a low degree of constraint violation.

First, we define the penalty term for dispersion violation. Let

$$\ell_{i,j} = \max\{0, 2D - d(c_i, c_j)\}, \quad (3.1)$$

hence we get $\ell_{i,j} = 0$ if and only if $d(c_i, c_j) \geq 2D$. There-

fore the total pairwise dispersion penalty $\sum_{i=1}^{p-1} \sum_{j=i+1}^p \ell_{i,j}^2$

equals 0 if and only if all the dispersion points are sufficiently far from each other. By Rademacher's Theorem [18], since d is continuous, $\ell_{i,j}^2$ is differentiable almost-everywhere for all i, j .

Second, before we define the boundary constraint term, we need two auxiliary definitions which are three-dimensional analogues of the definitions presented by Lai et al. [6]:

Active Face: Consider a polyhedral container C with a face F and a point c . Orient the normal vector N_F of face F inwards and denote $p \in F$ as the point in which N_F originates from. A face F is active with respect to c if either $c \in C$ and $N_F \cdot (c - p) \geq 0$ or if $c \notin C$ and $N_F \cdot (c - p) < 0$.

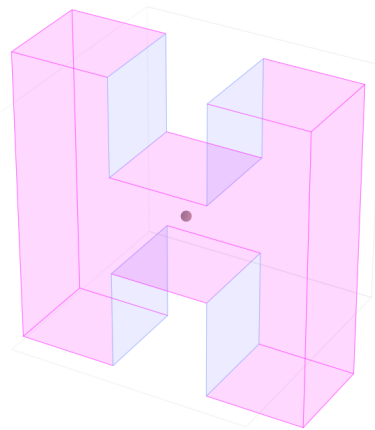


FIG. 1: All active faces (magenta) of the H-box container for point $c = (1.5, 0.5, 1.5)$ inside the container.

Fig. 1 depicts the active faces for a point inside the H-shaped container, and Fig. 2 depicts the active faces for a point outside the H-shaped container. An active face can be thought of as an oriented plane that is geometrically relevant to the point c . If c lies inside the polyhedron, then only the faces whose inward-normals

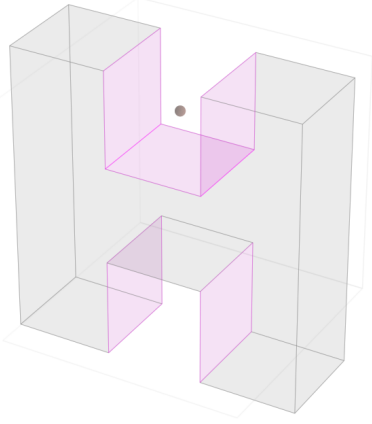


FIG. 2: All active faces (magenta) of the H-box container for point $c = (1.5, 0.5, 2.5)$ outside the container.

minimally constrain how close c is to the boundary of the container constitute the set of active faces. Alternatively, if c lies outside the boundary of the polyhedron, an active face is blocking c from entering the polyhedron. Active faces will contribute to the boundary constraint in the feasibility-residual function.

Active Footpoint: Consider a dispersion point c and an active face F of the container C . The *foot* h is the projection of c onto the plane P defined by the normal of F . We define h to be an *active footpoint* with respect to F if h lies on F . We denote H^i to be the set of all active footpoints with respect to the dispersion point c_i .

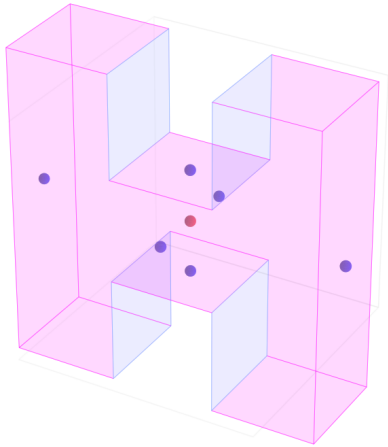


FIG. 3: All active footpoints (blue) inside the H-box container with respect to (red) point $(1.5, 0.5, 1.5)$ inside container with activate faces highlighted in pink.

Fig. 3 depicts a case where the footpoints of a dispersion point are all active. Fig. 4 depicts a case where not all footpoints of a dispersion point are active. The active footpoint h of a dispersion point c allows us to measure

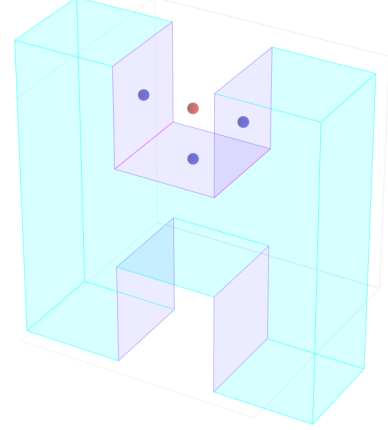


FIG. 4: All active footpoints (blue) inside the H-box container with respect to (red) point $(1.5, 0.5, 2.5)$ outside container with active faces highlighted in purple.

distances between dispersion points and the minimally relevant planes of the container, thereby providing a reference for the distance between a dispersion point and the container's boundary. When this perpendicular projection falls directly on the face F , F is the boundary face that governs how close c may move toward the container's boundary, and the point-to-face distance is determined by the separation between c and this footpoint.

Orientation equips the polyhedron with coherent inward normals, making the active face selection rule an orientation-consistent generalization of the counterclockwise active-edge mechanism used in the planar formulation [6]. Unlike the two-dimensional case, where the boundary is a closed, non-self-intersecting loop of segments with an inherent cyclic ordering, the boundary of a three-dimensional container forms a polyhedral complex with no analogous ordering. The extension from active edges [6] to active faces and their associated footpoints provides the geometric machinery needed to generalize boundary interactions from vertices and edges in two dimensions to vertices, edges, and faces in three dimensions. Thus, active faces constitute the minimal and geometrically natural extension of the active-edge concept from two to three dimensions, enabling a unified treatment of boundary constraints in arbitrary polyhedral domains.

Now, we define the boundary penalty for a dispersion point c_i as

$$O_i = \begin{cases} D + 2 \cdot (\min\{d(c_i, v) : v \in V \cup H^i\})^2 & c_i \notin C, \\ \sum_{v \in V \cup E \cup H^i} (\max\{0, D - d(c_i, v)\})^2 & c_i \in C. \end{cases} \quad (3.2)$$

When $c_i \in C$, the boundary penalty is equal to the sum of all the squared distances between c_i and the vertices, edges, and faces of the container in which the c_i is at most D away. In particular, given the open ball $B_D^o(c_i)$ of radius D centered at c_i , each vertex, edge, and active foot-

point of the container which has a non-empty intersection with $B_D^o(c_i)$ will contribute to the boundary penalty term O_i . If the distance to any vertex, edge, or footpoint from the dispersion point c_i is larger than D , then no penalty is contributed. When $c_i \notin C$, a penalty is still imposed as the dispersion point is located outside the bounds of the container. In such a case, the minimum distance to a vertex or footpoint of the container is used as a basis for the penalty term. We add D to this penalty term so that for points located outside the container, the boundary penalty term is always positive, and the penalty increases with D .

We now define the energy function $E : (\mathbb{R}^3)^p \times \mathbb{R} \rightarrow \mathbb{R}$ where $D > 0$ is fixed and $X = (c_1, \dots, c_p) \in (\mathbb{R}^3)^p$ by

$$E(X, D) = \sum_{i=1}^{p-1} \sum_{j=i+1}^p \ell_{i,j}^2 + \sum_{i=1}^p O_i. \quad (3.3)$$

The first term of Equation 3.3 deals with the dispersion constraint, or constraint (ii), of the CpDP. Recall, the first term of Equation 3.3 is identically zero if and only if $d(c_i, c_j) \geq 2D$ for all distinct $i, j \in [p]$. When D is fixed, we write $E_D(X) := E(X, D)$. Additionally, the second term deals with the containment constraint and the boundary constraint, or constraints (i) and (iii), respectively. Note, O_i is zero if and only if $c_i \in C$ and $d(c_i, \partial C) \geq D$. Therefore, it is worth noting that $E_D(X)$ is identically zero if and only if for a fixed $D > 0$, the configuration $X = \{c_1, \dots, c_p\}$ is a feasible solution to the nonlinear optimization problem.

Equation 3.3 gives a feasibility-residual function which lifts the optimization model proposed by Lai et al. [6] from two dimensions into three dimensions. Not only does it cleanly describe a feasibility-residual function for any polyhedral container, but is also differentiable almost-everywhere. The advantage of such a function allows one utilize gradient-based solvers (i.e., L-BFGS [15]) to find feasible solutions for a fixed $D \geq 0$ from initial random configurations.

IV. GLOBAL OPTIMIZATION ALGORITHM

In this section we propose our global optimization algorithm which builds upon the framework introduced by Lai et al. [6]. The global optimization process is structured as a multi-start pipeline to navigate the complex, non-convex solution space. In each global iteration, the algorithm restarts by generating an initial random configuration of p points uniformly distributed within the polyhedral container. This multi-start approach is necessary because the problem's non-smooth objective function and numerous distance constraints frequently trap standard optimization tools in poor local optima [5]. As shown in Fig. 5, within each iteration, the Tabu Search procedure acts as a feasibility solver by minimizing the feasibility-residual function 3.3 to find a valid configuration given a fixed min-

imum distance D . Once a feasible configuration is found, a distance adjustment procedure applies the Sequential Unconstrained Minimization Technique (SUMT) [19] to iteratively maximize D while preserving the feasibility of the configuration.

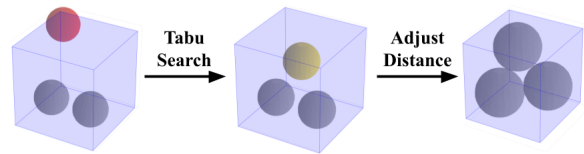


FIG. 5: Overview of the global optimization algorithm. The process demonstrates a two-stage approach: first, Tabu Search is employed to relocate a candidate sphere (red) from an initial, infeasible position to a feasible position (yellow). Second, an Adjust Distance phase maximizes the uniform radius of all spheres to achieve an optimal packing configuration.

A. Tabu Search

We employ a Tabu Search procedure [10], following the framework used by Lai et al. [6]. Tabu Search is a combinatorial heuristic designed to escape poor local configurations (high-energy) and move the system toward a better (lower-energy) arrangement of dispersion points inside the container. The core principle behind the Tabu Search is the *tabu list* which maintains a short term list of recent moves that are temporarily forbidden in subsequent iterations [10]. The tabu list ensures the algorithm does not fall into cycles of re-evaluating configurations. If the tabu list has reached its maximum allowable size, then the least recent addition to the tabu list is removed.

The Tabu Search heuristic incentivizes long-term exploration of the solution space. The maximum number of successive moves the algorithm is allowed to explore without improving from the initial configuration is specified by a parameter β . If Tabu Search makes β iterations without improving on the last-improved configuration, then the procedure terminates. A small β enables a quicker Tabu Search, but only scans for solutions which are a few moves different from the initial configurations. A large β enables a deeper scan of neighboring solutions, but forces a longer runtime for Tabu Search. Tabu Search proves to be a powerful tool for efficiently scanning families of solutions using combinatorial optimization methods on a continuous region and transforming high-energy configurations to low-energy configurations.

For a given configuration $X = \{c_1, \dots, c_p\}$, we quantify the *energy of a point* by the degree to which it violates the dispersion and boundary constraints. We define the energy of a dispersion point c_i as

$$E_D(c_i) = \sum_{j \neq i} \ell_{i,j}^2 + O_i \quad (4.1)$$

where $\ell_{i,j}$ is the dispersion penalty term and O_i captures the boundary violation term as in Equation 3.2. To propose new candidate positions for dispersion points, we consider *vacancy sites*, which are random locations inside the container not currently occupied by a dispersion point. A vacancy site c has energy

$$E_D(c) = \sum_{i=1}^p \ell_{c,j}^2 + O_c \quad (4.2)$$

where $\ell_{c,j}$ replaces c_i with c in Equation 3.1 and O_c replaces c_i with c in Equation 3.2. Vacancy sites with low energy represent positions that are more compatible with the current configuration, i.e., points where it would be the “easiest” to insert another ball.

A *neighbor* X_{nb} of a solution X can be found by *moving* a single dispersion point of X to a new location. The *neighborhood* $N(X)$ is the set of neighbors of X . To select the most promising neighbor of a given configuration X , we sample $N(X)$ by identifying the Q highest-energy dispersion points and the Q lowest-energy vacancy sites selected from a pool of $10p$ randomly generated candidates, where p is the total number of dispersion points. While Lai et al. [6] suggest generating only $5p$ vacancy sites, we increased this sample size to $10p$ to maintain sufficient search breadth, compensating for the lower sampling density inherent in three-dimensional space compared to two. We analyze the possible moves between these sets to identify the pairing that offers the best potential reduction in energy.

For a specific dispersion-vacancy move, the resulting configuration is merely a rough approximation of a feasible solution. Since vacancy sites are generated randomly, simply placing a point at one of these coordinates rarely resolves the feasibility-residual value, defined in Equation 3.3, to zero. Therefore, we do not evaluate the quality of this raw move directly. Instead, we pass this intermediate configuration to our local optimization subroutine, LOCALOPT. LOCALOPT serves as the mandatory bridge between the discrete combinatorial search and the continuous solution space. It utilizes a gradient-based solver, specifically the Limited-memory Broyden-Fletcher-Goldfarb-Shanno (L-BFGS) algorithm [15], to drive the rough candidate configuration toward the nearest smooth minimum of the energy function. Consequently, the Tabu Search algorithm never compares unrefined moves; it strictly compares the *locally optimized* outcomes of those moves to decide if a step is an improvement.

However, even with this precise local refinement, the global solution space of Equation 3.3 remains non-convex and populated with numerous local minima [6]. To prevent the algorithm from becoming trapped in the first deep valley it encounters, we integrate Monotonic Basin Hopping (MBH) as a heuristic for global exploration, as suggested by Lai et al. [6]. Unlike Tabu Search, which evolves a solution along a specific path, MBH samples the global landscape by “hopping” between independent basins (i.e., regions converging to a single minimum) [20].

It operates by taking a solution (X, D) , performing random perturbations to jump into a neighboring basin, and then applying LOCALOPT. The new local minimum is accepted only if it offers a strict improvement, ensuring the system can escape shallow local optima in search of a global minimum.

Algorithm 1 Tabu Search

Require: C (Container), X (configuration), $D \in \mathbb{R}_{>0}$, $\beta \in \mathbb{Z}_{>0}$, $Q \in \mathbb{Z}_{>0}$, $\epsilon \in \mathbb{R}_{>0}$

- 1: $Q \leftarrow \min\{Q, p\}$
- 2: $X \leftarrow \text{LOCALOPT}(X, D)$
- 3: $X^{\text{best}} \leftarrow X$, $NoImprove \leftarrow 0$, $TabuList \leftarrow \{\}$
- 4: **while** $NoImprove \leq \beta$ and $E_D(X_{\text{best}}) > \epsilon$ **do**
- 5: $p_1, \dots, p_Q \leftarrow \text{HIGHENERGYPOINTS}(X, D, Q)$
- 6: $q_1, \dots, q_Q \leftarrow \text{VACANCYSITES}(X, D, Q)$
- 7: $X_{\text{nb}}^{\text{best}} \leftarrow \text{MOVEPOINT}(X, p_1, q_1)$
- 8: **for** $(i, j) \in [Q] \times [Q]$ **do**
- 9: $X_{\text{nb}} \leftarrow \text{MOVEPOINT}(X, p_i, q_j)$
- 10: $X_{\text{nb}} \leftarrow \text{LOCALOPT}(X_{\text{nb}}, D)$
- 11: **if** $\text{MOVE}(p_i, q_j)$ not forbidden **then**
- 12: $X_{\text{nb}}^{\text{best}} \leftarrow X_{\text{nb}}$ if $E_D(X_{\text{nb}}) < E_D(X_{\text{nb}}^{\text{best}})$
- 13: $BestMove \leftarrow \text{MOVE}(p_i, q_j)$
- 14: **end if**
- 15: **end for**
- 16: $X \leftarrow X_{\text{nb}}^{\text{best}}$
- 17: Update $TabuList$ with $BestMove$
- 18: $X \leftarrow \text{MBH}(X, D)$
- 19: **if** $E_D(X) < E_D(X^{\text{best}})$ **then**
- 20: $X^{\text{best}} \leftarrow X$
- 21: $NoImprove \leftarrow 0$
- 22: **else**
- 23: $NoImprove \leftarrow NoImprove + 1$
- 24: **end if**
- 25: **end while**
- 26: **return** X^{best}

Algorithm 1 outlines the Tabu Search procedure. To visualize the effect of Tabu Search, Fig. 6 illustrates a candidate move for a fixed radius D within a cubic container.

The dispersion point shown in red is in a high-energy state due to a boundary constraint violation (protrusion from the container). The yellow sphere represents a randomly generated vacancy site located in a feasible region. The red arrow indicates the proposed movement: displacing the violating particle to this vacancy site. In this specific example, because the target site satisfies all constraints (it is inside the boundary and non-overlapping), the feasibility-residual value is zero. Consequently, the subsequent LOCALOPT routine will confirm this new configuration as stable with minimal. To prevent cycling, the algorithm explicitly forbids the reverse move in future iterations; the yellow dispersion point is temporarily restricted from returning to the high-energy neighborhood of the red sphere. This demonstrates the primary function of Tabu Search: executing coarse, global jumps to

locate feasible regions, which are then refined by local optimization.

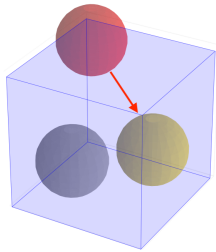


FIG. 6: **Visualization of a candidate neighbor generation.** The red sphere represents the point selected for movement (e.g., a high-energy point). The red arrow indicates the proposed displacement vector, targeting the location currently occupied by the yellow sphere.

B. Adjust Distance

After the Tabu Search procedure is completed, the resulting configuration X is a feasible solution, but typically not optimal. To find the nearest optimal solution X^* for the given configuration X , we employ the Sequential Unconstrained Minimization Technique (SUMT) [19] as proposed by Lai et al. [6] to convert the original CpDP (as a constrained optimization problem) into a sequence of unconstrained optimization problems and solve each until a feasible local minimum solution is found. Each unconstrained subproblem can be expressed as

$$\text{Minimize } \Phi_\mu(X, D) = -D^2 + \mu \times E(X, D) \quad (4.3)$$

where X is a candidate solution, D is the radius of the solution X , μ is the penalty factor to define the unconstrained optimization problem.

Algorithm 2 is the method to adjust a feasible configuration from Algorithm 1 into a local optimum. The distance adjustment method will iteratively minimize Equation 4.3 for strictly increasing values of μ . The $-D^2$ term in Equation 4.3 is to ensure that when we minimize this function, we promote maximizing D . Equation 3.2 contains $(\max\{0, D - d(c_i, v)\})^2$ which grows quadratically with D . The $-D^2$ term thus ensures Equation 4.3 is not dominated by $E(X, D)$ [6]. The distance adjustment procedure slightly adjusts the configuration X and the allowed minimum distance D through local optimization to find a local optimum of the original CpDP.

Algorithm 2 Adjust Distance

Require: X_0 (configuration), $D_0 \in \mathbb{R}_{>0}$, $K \in \mathbb{Z}_{>0}$

- 1: $X \leftarrow X_0$, $D \leftarrow D_0$, $\mu \leftarrow 10.0$
- 2: **for** $i \leftarrow 1$ to K **do**
- 3: $(X, D) \leftarrow \text{LOCALOPTPHI}(X, D, \mu)$
- 4: $\mu \leftarrow 5 \cdot \mu$
- 5: **end for**
- 6: **return** (X, D)

The LOCALOPTPHI function is a run of L-BFGS on the function Φ_μ from an initial solution (X_i, D_i) and penalty factor μ . Empirical results suggest that μ can be initialized to at most 100 so the gradient of Φ_μ is not ill-conditioned at the initial iteration, allowing for a local optima to be located in the initial iteration. Note, we do not call LOCALOPT in Algorithm 2, since D is fixed, hence minimizing $E_D(X)$ will not change D . Moreover, it would not help to call LOCALOPTPHI in Algorithm 1 since Tabu Search is only designed for finding feasible configurations for a fixed D . It is important not to “rush” finding a maximal value of D as finding a stable and feasible configuration X first often leads to a smoother maximization of D .

C. Global Optimization

The global optimization procedure is summarized in Algorithm 3. This algorithm represents a three-dimensional analogue to the TSGO framework established by Lai et al. [6]. While Lai et al. [6] utilized a time-bounded loop with continuous dependency on the global best state, our approach adopts an iterative multi-start strategy. This modification decouples the search trajectories, allowing each iteration to explore a distinct portion of the solution space independently before comparing against the current global optimum.

By shifting to an iteration-based structure, we ensure that the algorithm extensively samples the configuration space. Each iteration begins with a fresh randomization, preventing the solver from becoming trapped in a previously found local optimum. This is particularly crucial for non-convex containers where the feasible region may be disconnected.

Algorithm 3 Global Optimization

Require: $p \in \mathbb{N}$, C , D_{init} , N (number of iterations)

Ensure: Best configuration (X^*, D^*)

```

1:  $X \leftarrow \text{RANDOM\_SOLUTION}(p)$ 
2:  $X \leftarrow \text{TABU\_SEARCH}(X, D)$ 
3:  $X, D \leftarrow \text{ADJUST\_DISTANCE}(X, D, 15)$ 
4:  $X^*, D^* \leftarrow X, D$ 
5: for  $i = 1$  to  $N$  do
6:    $D_i \leftarrow D^*$ 
7:    $X_i \leftarrow \text{RANDOM\_SOLUTION}(p)$ 
8:    $X_i \leftarrow \text{TABU\_SEARCH}(X_i, D_i)$ 
9:   if  $E_{D_i}(X_i) < \varepsilon$  then
10:     $(X_i, D_i) \leftarrow \text{ADJUST\_DISTANCE}(X_i, D_i, 15)$ 
11:    if  $D_i > D^*$  then
12:       $X^*, D^* \leftarrow X, D$ 
13:    end if
14:  end if
15: end for
16: return  $(X^*, D^*)$ 

```

Within each iteration, the algorithm retains the rigorous local search operators utilized by Lai et al. [6]. An initial configuration is generated via `RANDOMSOLUTION`, followed by `TABUSEARCH` to locate the nearest local minimum. We then employ a strict feasibility check: only if the feasibility-residual value $E_D(X)$ for the configuration X falls below the tolerance threshold ε does the algorithm proceed to `ADJUSTDISTANCE`. This ensures that computational resources in the expensive refinement phase are reserved solely for valid, high-quality candidate solutions that have a genuine potential to improve upon the current global maximum D^* . At the local level, the optimization subroutines rely on a gradient-based solver governing Equation 3.3. This method exploits the specific geometry of the polyhedral container to achieve efficient convergence. Using gradient-based solvers over an almost-everywhere differentiable feasibility-residual function provides a smooth convergence path, offering greater stability than repulsion-based heuristics that rely on physical dynamical system simulations.

V. RESULTS AND EVALUATION

Experimentation is carried out on a personal computer with an Apple M2 Pro 3.5 GHz processor and 32GB RAM running on a 64-bit ARM-based MacOS 26.2. CPU times are given in seconds. The algorithm is implemented in Python 3.11, and the source code is publicly available (Source Code). Our specialized hybrid solver pairs Tabu Search with an L-BFGS optimizer to efficiently handle the problem’s $3p + 1$ variables and highly non-convex solution space, avoiding the local minima traps that stall standard generic solvers. We enforce a constraint violation tolerance of $\epsilon = 10^{-8}$ and truncate reported results to eight decimal places, ensuring the reported configurations are strictly feasible within the container geometry.

We evaluate our algorithm on five polyhedral containers of increasing geometric complexity: the unit cube, unit-length tetrahedron, H-shaped box, star-shaped polyhedron, and a ribbed ventilation cage. The boundaries for each are defined using a vectorized representation of inward-pointing normals for efficient distance calculations. To evaluate robustness, we benchmarked our algorithm against Packomania optima [21], best-known results from Kazakov et al. [7], and a computational baseline using the `scipy.optimize.differential_evolution` (DE) solver [22]. The DE baseline was configured with the `best1bin` mutation strategy, a population size factor of 15, a 2400-second time limit, and a hard penalty for boundary constraints.

Algorithm parameters scaled with the number of dispersion points (p). Global iterations were set to 1 for small instances ($p < 10$), 3 for medium ($10 \leq p < 30$), and 5 for large ($p \geq 30$). Tabu Search depth β was similarly scaled to 5, 10, and 15, respectively, with a tabu-rearrangement parameter of $Q = 3$ to align with Lai et al. [6]. The initial minimum distance D_{init} was 0.01 for small instances. For medium and large instances, D_{init} was calculated using an initial packing density of $\rho_{\text{init}} = 0.3$ to ensure active penalty terms without over-congestion [6, 23]:

$$D_{\text{init}} = \sqrt[3]{\frac{3 \cdot V_{\text{container}} \cdot \rho_{\text{init}}}{4\pi p}} \quad (5.1)$$

A. Cube

We benchmark our algorithm in the unit cube against analytical optima for $p \leq 10$ [11] and best-known configurations for $p > 10$ from Packomania [21]. We measure performance using absolute error ($A_{\text{err}} = D_{\text{Ours}} - D_{\text{Best}}$) and relative error ($R_{\text{err}} = A_{\text{err}}/D_{\text{Best}} \times 100\%$).

Table I demonstrates high numerical accuracy. The algorithm consistently reaches the theoretical optimum for small instances ($p \leq 10$, excluding $p = 7$) and high-symmetry cases like $p = 27$ ($< 0.0001\%$ error). Despite the increasingly non-convex search space, R_{err} for larger instances ($p = 20$ to 60) remains largely within 1%, with slight error increases at $p = 21$ and $p = 50$ likely indicating a high density of local optima. Furthermore, Fig. 9 confirms our method closely tracks theoretical values across all tested ranges, whereas the DE baseline’s performance degrades rapidly as p increases.

To illustrate the algorithm’s versatility across different geometries, we present visualizations in Fig. 7 and Fig. 8 under the Euclidean and ℓ_∞ (sup-norm) metrics for packing ten points. The ℓ_∞ metric is particularly relevant as its geometry aligns with the rectilinear boundaries of the unit cube. As seen in Fig. 8, the algorithm effectively handles the flat-edged “spheres” of the sup-norm, achieving a configuration that is remarkably close to the theoretical optimum ($D^* = \frac{1}{6}$).

TABLE I: Comparison of achieved minimum distances D_{Ours} with optimal values D_{Best} for $p = 1, \dots, 60$ in the unit cube (Euclidean metric).

p	D_{Ours}	D_{Best}	A_{err}	$R_{\text{err}}(\%)$
1	0.50000000	0.50000000	0.00000000	0.0000%
2	0.31698729	0.31698730	-1.0×10^{-8}	-0.0000%
3	0.29289321	0.29289322	-1.0×10^{-8}	-0.0000%
4	0.29289321	0.29289322	-1.0×10^{-8}	-0.0000%
5	0.26393200	0.26393202	-2.0×10^{-8}	-0.0000%
6	0.25735926	0.25735931	-5.0×10^{-8}	-0.0000%
7	0.25009464	0.25013615	-4.2×10^{-5}	-0.0166%
8	0.24999999	0.25000000	-1.0×10^{-8}	-0.0000%
9	0.23205080	0.23205081	-1.0×10^{-8}	-0.0000%
10	0.21428565	0.21428571	-6.0×10^{-8}	-0.0000%
20	0.17840693	0.17840720	-2.7×10^{-7}	-0.0002%
21	0.17521516	0.17721904	-2.0×10^{-3}	-1.1307%
27	0.16666660	0.16666667	-7.0×10^{-8}	-0.0000%
30	0.16018841	0.16018862	-2.1×10^{-7}	-0.0001%
40	0.14553682	0.14705882	-1.5×10^{-3}	-1.0350%
50	0.13426749	0.13595451	-1.7×10^{-3}	-1.2409%
60	0.12948983	0.13060194	-1.1×10^{-3}	-0.8515%

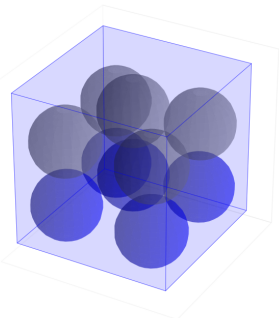


FIG. 7: Best-achieved 10-point configuration for the p -dispersion problem in the unit cube using the Euclidean metric ($D = 0.214285$).

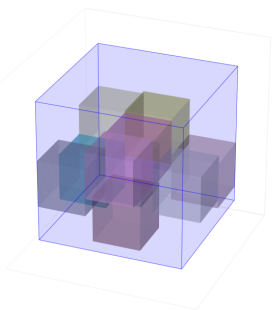


FIG. 8: Best-achieved 10-point configuration for the p -dispersion problem in the unit cube using the ℓ_∞ metric ($D = 0.166666$).

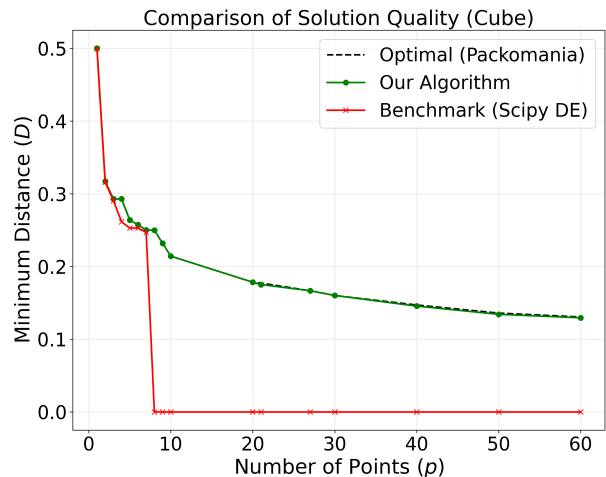


FIG. 9: Performance comparison in the unit cube showing the best minimum distance D for the proposed TSGO algorithm, the baseline DE solver, and the theoretical optima for p points.

B. Tetrahedron

We benchmark our algorithm against the best-known results for p -dispersion in the unit tetrahedron reported by Kazakov et al. [7] for $p = 1, \dots, 10$. Additionally, we report on our best-achieved minimum distances for $p = 20, 35, 56$ being the subsequent tetrahedral numbers. Kazakov et al. [7] mention that for three-dimensional space, the computational complexity of their algorithm increases significantly; hence they did not report on instances for $p > 10$. We execute our global optimization algorithm using the same parameters as in previous sections the packing density-based initialization ($\rho_{\text{init}} = 0.3$) for higher values of p . While Kazakov et al. [7] report results up to five decimal places, we report our results truncated to eight decimal places to maintain consistency with other sections of this paper.

Table II presents the absolute difference $A_{\text{err}} = D_{\text{Ours}} - D_{\text{Benchmark}}$ and the relative percentage improvement R_{err} between our solution and the benchmark. As shown in the table, our algorithm consistently identifies packing configurations with equal or strictly larger minimum pairwise distances than Kazakov et al. [7].

To further analyze these improvements, Fig. 10 illustrates the performance comparison between our algorithm, the results by Kazakov et al. [7], and the DE solver. While the `scipy.optimize.differential_evolution` baseline remains competitive for $p \leq 8$, its performance degrades sharply for $p \geq 9$, with the error gap spiking significantly as the solver fails to navigate the increasingly complex configuration space. Fig. 11 provides a visual comparison of the best configuration found by our algorithm against the corresponding configuration derived from the parameters in Kazakov et al. [7] for $p = 9$.

The results demonstrate that our proposed method

TABLE II: Comparison of our achieved minimum distances (D_{Ours}) against the best-known values ($D_{\text{Benchmark}}$) from Kazakov et al. [7] for the unit tetrahedron.

p	D_{Ours}	$D_{\text{Benchmark}}$	A_{err}	$R_{\text{err}}(\%)$
1	0.20412415	0.20045	0.00367415	+1.8330%
2	0.14494897	0.14204	0.00290897	+2.0480%
3	0.14494896	0.14204	0.00290896	+2.0480%
4	0.14494896	0.14204	0.00290896	+2.0480%
5	0.12247447	0.12147	0.00100447	+0.8269%
6	0.11387067	0.11243	0.00144067	+1.2814%
7	0.11237234	0.11062	0.00175234	+1.5841%
8	0.11237238	0.10600	0.00637238	+6.0117%
9	0.11237238	0.10250	0.00987238	+9.6316%
10	0.11237236	0.10200	0.01037236	+10.1690%
20	0.09175157	–	–	–
35	0.07752526	–	–	–
56	0.06190401	–	–	–

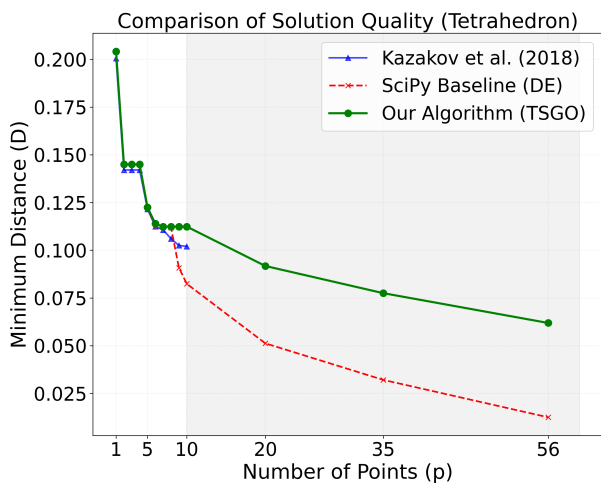
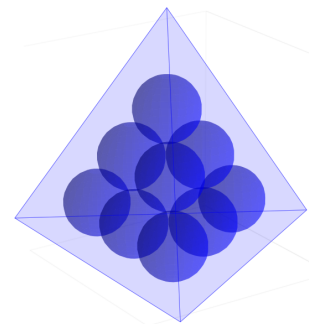


FIG. 10: Performance comparison in the unit tetrahedron showing the best minimum distance D for the proposed TSGO algorithm, the baseline DE solver, and the benchmarks from Kazakov et al. [7].

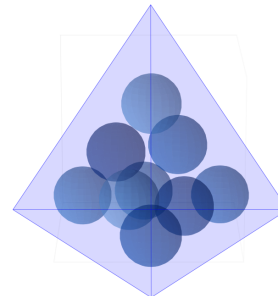
consistently outperforms both the existing literature and standard computational baselines. We achieve a minimum improvement of approximately 0.8% for all tested values of p compared to Kazakov et al. [7], with the performance gap widening to over 10% as p reaches the limits of the previously reported benchmarks.

C. H-Box

Non-convex containers, such as the H-shaped polyhedron, present significant geometric challenges for the CpDP. Unlike convex domains, non-convex shapes often feature disconnected feasible regions and obstructed lines of sight, where the straight-line segment connecting two



(a) Our best-achieved configuration for $p = 9$ ($D = 0.11237238$).



(b) Feasible packing for $p = 9$ using the radius ($D = 0.1025$) from Kazakov et al. [7].

FIG. 11: Visual comparison of packing density for 9 dispersion points in the unit tetrahedron. Our method (a) achieves a significantly tighter packing than the benchmark parameters (b).

valid points may pass through the infeasible exterior [5]. These characteristics create numerous “trapped” local minima that can stall standard optimization algorithms [6]. The H-shaped polyhedron was created with inspiration from its two-dimensional analogue: the H-shaped polygon [5].

To evaluate the performance of our algorithm, we compared our results against the SciPy DE solver. Table III compares the best minimum distances (D_{Ours}) achieved by our algorithm against this baseline (D_{Baseline}) for $p = 1, \dots, 60$ points under the Euclidean metric. We report the absolute improvement $A_{\text{err}} = D_{\text{Ours}} - D_{\text{Baseline}}$ and the relative percentage improvement R_{err} .

The results demonstrate a stark performance gap between the two methods. While the baseline solver remains competitive for $p \leq 7$, it fails to report a nontrivial configuration for larger values of p , configurations in which the minimum distance is $D = 0.0$. In contrast, our proposed algorithm successfully identifies high-quality solutions across the entire range, maintaining structural feasibility even at high packing densities.

To validate the performance of our method in these non-convex domains, Fig. 12 illustrates the best minimum distance (D) achieved by each solver. The divergence highlights the baseline’s inability to navigate the narrow

TABLE III: Comparison of achieved minimum distances for the H-shaped box (D_{Ours}) against the Differential Evolution baseline (D_{Baseline}).

p	D_{Ours}	D_{Baseline}	A_{err}	$R_{\text{err}}(\%)$
1	0.50000001	0.49999742	+0.00000259	+0.001%
2	0.50000000	0.49999183	+0.00000817	+0.002%
3	0.50000000	0.49997360	+0.00002640	+0.005%
4	0.50000000	0.49997731	+0.00002269	+0.005%
5	0.50000000	0.49996936	+0.00003064	+0.006%
6	0.50000000	0.49938900	+0.00061100	+0.122%
7	0.50000000	0.47443668	+0.02556332	+5.388%
8	0.41093592	0.27026219	+0.14067373	+52.051%
9	0.39725847	0.36077084	+0.03648763	+10.114%
10	0.39360889	0.22369906	+0.16990983	+75.955%
20	0.30427141	0.00000000	+0.30427141	∞
30	0.28046438	0.00000000	+0.28046438	∞
40	0.26696214	0.00000000	+0.26696214	∞
50	0.24122813	0.00000000	+0.24122813	∞
56	0.24999983	0.00000000	+0.24999983	∞
60	0.19986383	0.00000000	+0.19986383	∞

passages and internal corners of the H-box, while our algorithm remains robust.

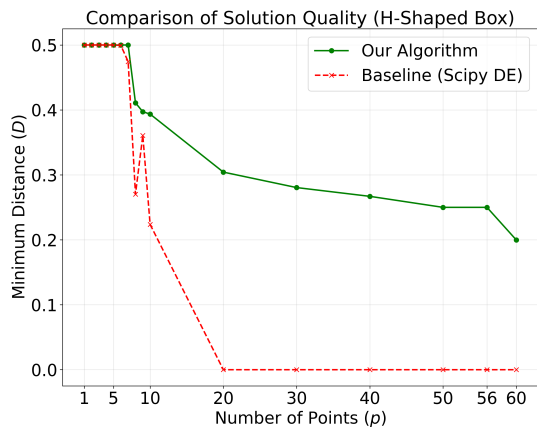


FIG. 12: Performance comparison on the H-shaped box. The baseline solver (red) fails completely for $p \geq 20$ ($D = 0$), whereas our algorithm (green) effectively explores the non-convex passage to maintain non-trivial separation distances.

Fig. 13 visualizes the best-achieved configuration for $p = 56$ points. This high-density packing illustrates the algorithm’s ability to maintain structural stability across non-convex junctions. Notably, the spheres form a coordinated “bridge” through the central passage while maintaining a rigid structure in the lateral segments, effectively utilizing the restricted volume to achieve $D \approx 0.25$. This configuration confirms that our Tabu Search method effectively navigates the disconnected feasible regions that typically obstruct global optimizers.

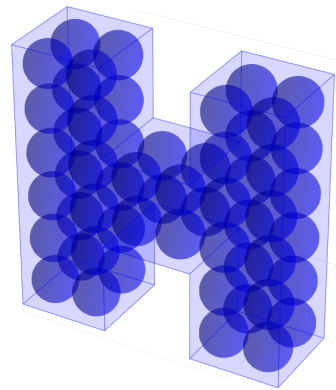


FIG. 13: Best achieved configuration of $p = 56$ dispersion points within the non-convex H-shaped container ($D = 0.24999983$). The visualization highlights the algorithm’s ability to resolve tight packing constraints within narrow, non-convex passages.

D. Star-Shaped Polyhedron

The star-shaped polyhedron draws inspiration from the Kepler-Poinsot polyhedron [24] and serves as a rigorous test case for non-convex optimization due to its distinctive central convex core connected to six narrow, tapering spikes. This originally developed geometry creates significant “bottlenecks” between the feasible sub-regions, making it difficult for optimization algorithms to migrate points from one spike to another. Unlike convex containers where local descent directions are often globally informative, the star-shaped polyhedron requires an algorithm capable of traversing infeasible space to escape the local optima found within individual spikes.

In Table IV, we report the best minimum distances (D_{Ours}) achieved by our algorithm for a range of p values. To demonstrate the scalability of our approach on highly constrained non-convex domains, we report results for large-scale instances up to $p = 100$.

TABLE IV: Achieved minimum distances for the star-shaped polyhedron (D_{Ours}).

p	D_{Ours}	p	D_{Ours}
1	1.41421356	9	0.72337216
2	0.97597051	10	0.69809740
3	0.90296401	20	0.57376175
4	0.90296402	30	0.49246630
5	0.90296400	40	0.45625711
6	0.90296396	50	0.39072828
7	0.81657905	60	0.36665003
8	0.76614274	100	0.33677304

The results indicate that our algorithm effectively exploits the available volume even as the number of points increases. For $p = 1$, the algorithm identifies the globally optimal placement within the central core. As p increases

to 6, the algorithm successfully distributes points into the six available spikes, maintaining a high separation distance of $D \approx 0.9029$. Beyond $p = 7$, crowding effects force a gradual reduction in the minimum distance D as the central core and spikes become filled.

Fig. 14 visualizes the best-achieved configuration for $p = 100$. This result is particularly notable as it demonstrates the algorithm’s capability to pack dispersion points uniformly into the tapering extremities of the spikes. Such regions are typically inaccessible to standard gradient-based solvers due to the narrow feasible widths and the high likelihood of points becoming trapped in local optima near the spike tips. The ability of our Tabu Search hybrid to relocate points across the non-convex “bottlenecks” is evidenced by the high packing density achieved in all six spikes simultaneously.

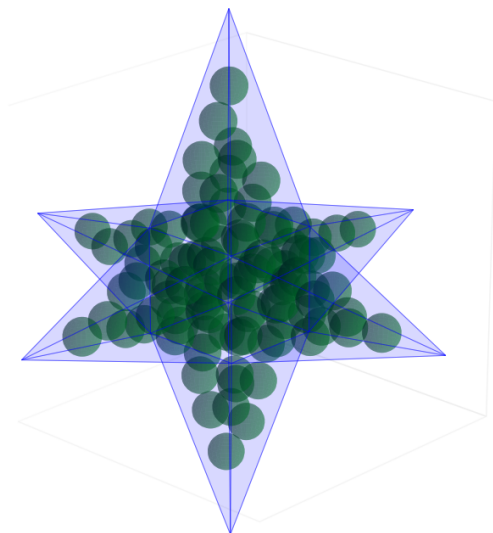


FIG. 14: Best achieved configuration of $p = 100$ dispersion points within the star-shaped container ($D = 0.33677304$).

E. Ribbed Ventilation Cage

Finally, we apply our algorithm to the “ribbed ventilation cage,” a highly complex non-convex polyhedron designed to model modern industrial computer casings and heat sinks. Unlike the H-shaped box or Star-shaped polyhedron, which feature large distinct sub-regions, this container is characterized by numerous corridors and separated legs. The inclusion of numerous internal pillars and ribs creates a “maze-like” feasible region, introducing frequent discontinuities that pose severe challenges for traditional gradient-based nonlinear optimizers.

The particular design of this ribbed ventilation cage polyhedral container is original, although the complexity

is practically motivated. In thermal engineering, components utilize ribbed structures, fins, and microstructures to maximize surface area and improve heat dissipation capabilities [25]. Solving the CpDP on such a geometry is therefore relevant for optimizing the layout of sensors, cooling pipes, or modular components within densely packed electronic enclosures. We evaluate our algorithm using both the Euclidean metric (ℓ_2), representing standard spherical component packing, and the sup-norm (ℓ_∞), which is critical for modeling the placement of cubic or box-shaped components often found in hardware design.

Fig. 15 and Fig. 16 visualize the results of our algorithm for dispersing $p = 50$ points with respect to the Euclidean metric and $p = 100$ points with respect to the ℓ_∞ metric within this highly constrained environment.

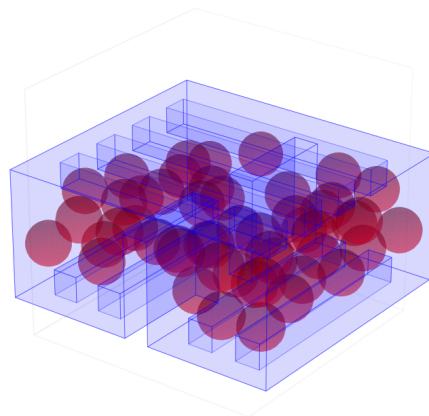


FIG. 15: Best achieved configuration for $p = 50$ points using the Euclidean metric ($D = 0.8247$).

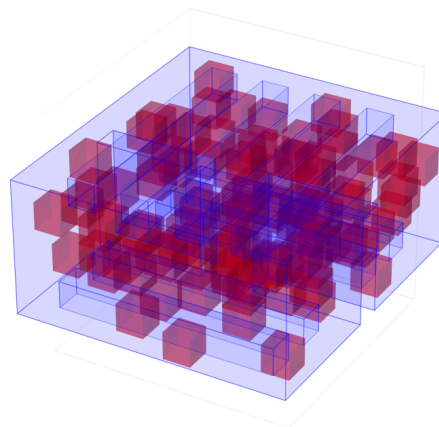


FIG. 16: Best achieved configuration for $p = 100$ points using the ℓ_∞ metric ($D = 0.4999$).

The successful dispersion of $p = 50$ points in this environment demonstrates the robustness of our approach. Despite the numerous internal obstacles that fracture the

search space, the algorithm achieves a uniform distribution, effectively utilizing the narrow corridors between pillars. This result validates the algorithm’s capability to handle large-scale dispersion problems ($p \geq 50$) within containers that exhibit both macro-scale non-convexity and micro-scale geometric obstructions.

F. Computational Efficiency and Scalability

To evaluate scalability, we recorded the wall-clock runtime required to converge to a feasible solution ($\varepsilon = 10^{-8}$). Fig. 17 compares runtimes across four container geometries (excluding the ribbed cage, where complex boundary checks overwhelmingly dominate).

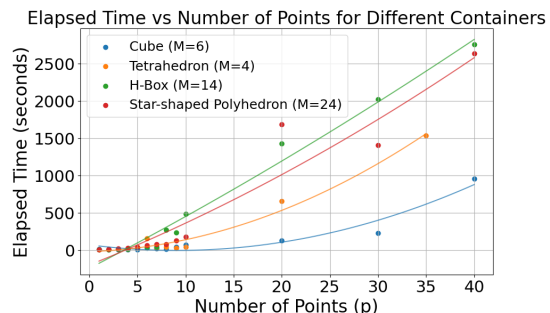


FIG. 17: **Comparative runtime analysis.** Runtime (seconds) versus dispersion points p . Solid lines indicate quadratic regression fits.

The empirical data closely matches quadratic regression fits, aligning with the $\mathcal{O}(p^2)$ complexity of pairwise distance checks and $\mathcal{O}(p \cdot M)$ complexity of boundary checks, where M is the number of faces. For small instances ($p \leq 10$), convergence takes under 50 seconds—vastly outperforming the 2400-second Differential Evolution baseline, which frequently timed out on non-convex shapes.

As p increases, geometric complexity dictates the scaling coefficient. Simple shapes like the unit tetrahedron ($M = 4$) and cube ($M = 6$) exhibit shallow growth. Conversely, the star-shaped polyhedron ($M = 24$) scales more steeply due to severe bottlenecks and increased “Active Face” evaluations. Crucially, all geometries maintain polynomial scaling, avoiding the exponential explosion common in combinatorial approaches. Even for the highly complex star-shaped container at $p = 100$, the algorithm converges in a tractable $\sim 4,900$ seconds.

VI. CONCLUSION

This paper introduces a robust global optimization framework for the Continuous p -Dispersion Problem (CpDP) in three-dimensional polyhedral containers under any metric. By defining a differentiable feasibility-residual function and extending the Tabu Search algorithm [6], we

successfully transition from restrictive two-dimensional planar checks to a comprehensive three-dimensional formulation utilizing a ray-casting procedure and projection-based distance calculations to faces, edges, and vertices. Empirical evaluations confirm that our method matches analytical optima in standard shapes [11] and establishes new high-dispersion benchmarks for complex, non-convex polyhedra [7], offering a powerful tool for real-world applications such as robotic collision avoidance and facility layout [8, 9].

Because our energy formulation relies on dimension-independent vector operations, it provides a natural foundation for extension into n -dimensional spaces (\mathbb{R}^n). The primary adaptation required for higher dimensions is generalizing the geometric container representation, specifically determining how to precisely model $(n - 1)$ -dimensional bounding hyperplanes and extending the ray-casting validity checks. Furthermore, future work will focus on incorporating more sophisticated, non-planar geometries such as curved surfaces. While polyhedral distances currently utilize efficient orthogonal projections, curved boundaries require representations like spline patches or implicit surfaces, necessitating the development of computationally efficient distance evaluation methods that do not rely on closed-form projections.

ACKNOWLEDGEMENTS

The authors would like to thank Ram Padmanabhan for their valuable feedback and editorial assistance throughout the preparation of this manuscript.

-
- [1] Michael Kuby. Programming models for facility dispersion: The p-dispersion and maximum dispersion problems. *Geographical Analysis*, 19:315–329, 1987.
- [2] Zvi Drezner and Erhan Erkut. Solving the continuous p-dispersion problem using non-linear programming. *Journal of the Operational Research Society*, 46(4):516–520, 1995.
- [3] Christoph Baur and Sándor P. Fekete. Approximation of geometric dispersion problems. *Algorithmica*, 30(3):451–470, 2001.
- [4] Ronald L. Graham, Boris D. Lubachevsky, Kari J. Nurmela, and Patric R.J. Östergård. Dense packings of congruent circles in a circle. *Discrete Mathematics*, 181(1):139–154, 1998.
- [5] Zhengguan Dai, Kathleen Xu, and Melkior Ornik. Repulsion-based p-dispersion with distance constraints in non-convex polygons. *Annals of Operations Research*, 307(1):75–91, 2021.
- [6] Xiangjing Lai, Zhenheng Lin, Jin-Kao Hao, and Qinghua Wu. An Efficient Optimization Model and Tabu Search-Based Global Optimization Approach for the Continuous p-Dispersion Problem. *INFORMS Journal on Computing*, 37, 2024.
- [7] Alexander L. Kazakov, Anna A. Lempert, and Trungthanh T. Ta. The sphere packing problem into bounded containers in three-dimension non-euclidean space. *IFAC-PapersOnLine*, 51(32):782–787, 2018.
- [8] Alaa Z. Abdulghafoor and Efstathios Bakolas. Distributed coverage control of multi-agent networks with guaranteed collision avoidance in cluttered environments. *IFAC-PapersOnLine*, 54(20):771–776, 2021.
- [9] Vigneash Loganathan, Saminathan Veerappan, Premkumar Manoharan, and Bizuwork Derebew. Optimizing drone-based iot base stations in 6g networks using the quasi-opposition-based lemurs optimization algorithm. *International Journal of Computational Intelligence Systems*, 17:218, 2024.
- [10] Fred W. Glover and Manuel Laguna. *Tabu Search*. Springer, 1997.
- [11] Jonathan Schaer. On the densest packing of spheres in a cube. *Canadian Mathematical Bulletin*, 9(3):265–270, 1966.
- [12] Maxwell Rosenlicht. *Introduction to Analysis*. Dover Books on Mathematics. Dover Publications, 2012.
- [13] Mark de Berg, Otfried Cheong, Marc van Kreveld, and Mark Overmars. *Computational Geometry: Algorithms and Applications*. Springer, 3rd edition, 2008.
- [14] James R. Munkres. *Analysis on Manifolds*. Advanced Books Classics. Addison-Wesley, 1991.
- [15] Roger Fletcher. *Practical Methods of Optimization*. Wiley, 1987.
- [16] Wencheng Wang, Jing Li, and Enhua Wu. 2D point-in-polygon test by classifying edges into layers. *Computers & Graphics*, 29:427–439, 2005.
- [17] Denis Horvat. Ray-casting point-in-polyhedron test. 2012.
- [18] Lawrence C. Evans and Ronald F. Gariepy. *Measure Theory and Fine Properties of Functions*. CRC Press, revised edition, 2015.
- [19] Anthony V. Fiacco and Garth P. McCormick. Computational algorithm for the sequential unconstrained minimization technique for nonlinear programming. *Management Science*, 10(4):601–617, 1964.
- [20] Thomas Bäck, Christophe Foussette, and Peter Krause. *Contemporary Evolution Strategies*. Springer, 2013.
- [21] Eckard Specht. Packomania: The best known packings of equal circles/spheres in various containers. <http://www.packomania.com/>, 2026.
- [22] Pauli Virtanen, Ralf Gommers, Travis E. Oliphant, Matt Haberland, Tyler Reddy, David Cournapeau, Evgeni Burovski, Pearu Peterson, Warren Weckesser, Jonathan Bright, Stéfan J. van der Walt, Matthew Brett, Joshua Wilson, K. Jarrod Millman, Nikolay Mayorov, Andrew R. J. Nelson, Eric Jones, Robert Kern, Eric Larson, C J Carey, İlhan Polat, Yu Feng, Eric W. Moore, Jake VanderPlas, Denis Laxalde, Josef Perktold, Robert Cimrman, Ian Henriksen, E. A. Quintero, Charles R. Harris, Anne M. Archibald, Antônio H. Ribeiro, Fabian Pedregosa, Paul van Mulbregt, and SciPy 1.0 Contributors. SciPy 1.0: Fundamental Algorithms for Scientific Computing in Python. *Nature Methods*, 17:261–272, 2020.
- [23] H. Groemer. Some basic properties of packing and covering constants. *Discrete & Computational Geometry*, 1(2):183–193, 1986.
- [24] Harold S. M. Coxeter. Star polytopes and the schläfli function $f(\alpha, \beta, \gamma)$. *Elemente der Mathematik*, 44(2):25–36, 1989.
- [25] Xin Lu, Lu Wang, Liangbi Wang, and Yao Hu. Heat transfer enhancement of diamond rib mounted in periodic merging chambers of micro channel heat sink. *Micromachines*, 16, 2025.